Spectrochimica Acta Part A: Molecular and Biomolecular Spectroscopy 245 (2021) 118939

Contents lists available at ScienceDirect

Spectrochimica Acta Part A: Molecular and Biomolecular Spectroscopy

journal homepage: www.elsevier.com/locate/saa

Optical properties of organosilicon compounds containing sigma-electron delocalization by quasiparticle self-consistent *GW* calculations

Maria I.A. de Oliveira [a,b], Roberto Rivelino [a,c,*], Fernando de Brito Mota [a], Anelia Kakanakova-Georgieva [c], Gueorgui K. Gueorguiev [c,**]

[a] Instituto de Física, Universidade Federal da Bahia, 40210-340 Salvador, Bahia, Brazil
[b] Instituto Federal da Bahia, Campus Ilhéus, 45671-700 Ilhéus-Itabuna, Bahia, Brazil
[c] Department of Physics, Chemistry and Biology (IFM), Linköping University, 581 83 Linköping, Sweden

ARTICLE INFO

Article history:
Received 30 May 2020
Received in revised form 28 August 2020
Accepted 7 September 2020
Available online 12 September 2020

Keywords:
Optical properties
Persilastaffanes
Si-C-based optical tags
GW method

ABSTRACT

We investigate theoretically the electronic and optical absorption properties of two sub-classes of oligosilanes: (i) $Si(CH_3)_4$, $Si_4(CH_3)_8$, and $Si_8(CH_3)_8$ that contain Si dot, ring and cage, respectively, and exhibit typical Si—C and Si—Si bonds; and (ii) persilastaffanes $Si_7H_6(CH_3)_6$ and $Si_{12}H_6(CH_3)_{12}$, which contain extended delocalized σ-electrons in Si—Si bonds over three-dimensional Si frameworks. Our modeling is performed within the *GW* approach up to the partially self-consistent GW_0 approximation, which is more adequate for reliably predicting the optical band gaps of materials. We examine how the optical properties of these organosilicon compounds depend on their size, geometric features, and Si/C composition. Our results indicate that the present methodology offers a viable way of describing the optical excitations of tailored functional Si-C-based clusters and molecular optical tags with potential use as efficient light absorbers/emitters in molecular optical devices.

© 2020 The Author(s). Published by Elsevier B.V. This is an open access article under the CC BY-NC-ND license (http://creativecommons.org/licenses/by-nc-nd/4.0/).

1. Introduction

The use of silicon-carbon-based molecular clusters, complexes, nanoparticles, and quantum dots, as potential efficient light emitters, also called optical tags, has been much beneficial for the development of nanoscale sensing technology [1–3]. Indeed, the electronic properties of such optical tags may be tuned by controlling the size, backbone, and Si/C ratio in the composition of a Si-C-based system [4,5]. At the molecular level, a compelling for applications and electronically flexible class of compounds containing Si—C bonds are the silane derivatives [6]. Examples include the sub-class of cyclic silanes [6–10] and the sub-class of persilastaffanes [11], both of which represent natural candidates as stable and efficient emitters when subjected to prolonged irradiation [12]. Furthermore, a facile synthetic approach to obtain silicon cluster structures is provided by structural rearrangement reactions of oligosilanes [13], which is considered as a useful bottom-up method to fabricate Si-based semiconductor devices.

Research focused on cyclic silanes and caged oligosilanes is especially of interest because of their unique electronic structure, involving σ electrons of Si—Si bonds delocalized over three-dimensional (3D) silicon structures [14–17]. Although there is a similarity between organosilicon compounds and hydrocarbons, the Si—Si σ conjugation may readily lead to small band gaps in polycyclic oligosilanes [18]. Moreover, these molecules exhibit a skeletal structure related to bulk crystalline or amorphous silicon, which makes them eligible to be incorporated in tiny Si-based devices. Additionally, their optical properties, which can be easily tuned by varying number of Si atoms, rings or cages in the molecule, successfully compete with Si-based nanoparticles [19] designed for nano-optical device applications.

From a more fundamental viewpoint, addressing the optical properties of small Si-based clusters contributes to new knowledge on how the peculiar geometry and chemical bonding shape their properties. Following such research line, the photoluminescence properties of octasilacubane, a cubic Si_8 cluster [20], have been experimentally investigated, understood, and related to its strained cage framework. Indeed, the first species of octasilacubane has long been synthesized [21] and has been demonstrated to be stable in an inert atmosphere. Other related representative of oligosilanes containing a single Si ring is the octamethylcyclotetrasilane, which has previously been studied by employing gas electron diffraction techniques [22]. However, accurate theoretically calculated absorption spectra for these Si-C-based

* Correspondence to: R. Rivelino, Instituto de Física, Universidade Federal da Bahia, 40210-340 Salvador, Bahia, Brazil.
** Corresponding author.
E-mail addresses: rivelino@ufba.br (R. Rivelino), gueorgui.kostov.gueorguiev@liu.se (G.K. Gueorguiev).

https://doi.org/10.1016/j.saa.2020.118939
1386-1425/© 2020 The Author(s). Published by Elsevier B.V. This is an open access article under the CC BY-NC-ND license (http://creativecommons.org/licenses/by-nc-nd/4.0/).

molecules that attract growing interest for applications in nano-optics [4,5] are scarce in the literature. Only very limited experimental data on the emission spectra of some cubic Si-molecules has been made available so far [21,23].

In this paper, we carry out first principles calculations to investigate the electronic and optical absorption properties of organosilicon archetypes, as a function of their structural features and Si concentration. We include the screening of the Coulomb interactions at the microscopic level to determine their optical gaps [24,25]. Thus, we are aiming at a systematic and reliable theoretical modeling useful for describing the optical properties of larger Si-C-based clusters, with potential applications as molecular sensors. Firstly, we examine the cases of the $Si_x(CH_3)_y$ sub-class of oligosilanes, namely, $Si(CH_3)_4$, $Si_4(CH_3)_8$, and $Si_8(CH_3)_8$, containing Si dot, ring and cage, respectively, and exhibiting typical Si—C and Si—Si bonds [20–23]. Secondly, we consider the $Si_xH_6(CH_3)_y$ sub-class of oligosilanes or persilastaffanes; i.e., $Si_7H_6(CH_3)_6$, and $Si_{12}H_6(CH_3)_{12}$, which contain extended delocalized σ electrons in Si—Si bonds over 3D silicon frameworks [11,26].

2. Methods and calculations

The electronic energies and the relaxed structures of the oligosilanes studied here were obtained within the local spin-density approximation (LSDA) [27], as implemented in the VASP code [28–31]. Within this scheme, the PAW method [32,33] was employed with kinetic energy cutoff 742.5 eV for the oligosilanes [$Si(CH_3)_4$ and $Si_4(CH_3)_8$, and $Si_8(CH_3)_8$]; and 400 eV for the persilastaffanes [$Si_7H_6(CH_3)_6$, and $Si_{12}H_6(CH_3)_{12}$]. These stoichiometric formulas facilitate the direct evaluation of the Si/C ratio and the Si concentration in each of the molecules studied. During the geometry relaxation process of the isolated molecules, only the Γ point was sampled in the Brillouin zone (BZ) in cubic boxes with edge 17–20 Å until atomic forces become 0.01 eV/Å using an electronic energy convergence criterion of 10^{-5} eV. Using this protocol, all studied molecules except the largest of the persilastaffanes are separated from their longitudinal images by distance large enough to exclude any non-physical interaction. Only the largest persilastaffanes (exhibiting length of ~12 Å) are separated from their longitudinal images by ~4 Å at each side, which may result in a small non-physical interaction for the isolated molecule. However, the present choice of the box size is considered necessary and a good trade-off due to the number of bands used in the subsequent calculations.

The dynamic polarizabilities of the systems were determined within the random phase approximation (RPA), using the longitudinal approach, and including local field effects combined with the PAW method, as described in Ref. [34] and references therein. This formalism is sufficiently accurate to describe dielectric properties of molecular systems such those studied here, in addition to more sophisticated nonlocal Hamiltonians [34]. Hence, for the Kohn-Sham (KS) systems, the irreducible polarizability, P, can be obtained in the independent particle picture, χ^0, as $P = \chi^0 + \chi^0 f_{xc} P$, being f_{xc} the density-functional xc-kernel. The local field effects are included in the Hartree approximation. In the RPA calculations we consider 450 bands in average, until the limit of 20 eV. The frequency-dependent dielectric matrices were calculated after the total convergence of the ground state energy for each system. The imaginary part of the dielectric matrix was determined by a sum over states including the unoccupied KS states, while the real part was calculated via the usual Kramers-Kronig transformation [34].

Table 1
Calculated bond lengths for the relaxed $Si_x(CH_3)_y$ oligosilanes at the LSDA/PAW level of calculation. Experimental values are given in parentheses.

Compound	Si–C (Å)	Si–Si (Å)
$Si(CH_3)_4$	1.86 (1.877) [40]	–
$Si_4(CH_3)_8$	1.87 (1.893) [22]	2.34 (2.362) [22]
$Si_8(CH_3)_8$	1.87	2.37 (2.398) [20]

The many-body calculations that underlie the GWA are well established in Refs. [25, 35–37]. In the present approach, the quasiparticle (QP) energies and absorption spectra of the oligosilanes are also computed by employing the KS eigenfunctions and eigenvalues to construct the single-particle propagator, G, and the screened Coulomb potential, $W = \epsilon^{-1}V$, that enters the non-local self-energy, $\Sigma = iGW$ [26]. The main advantage of this scheme over other approaches, such as hybrid functionals in DFT, is the non-phenomenological inclusion of the screening. Following the scheme of Hybertsen and Louie [36], the LDA gap values were corrected from the single shot G_0W_0 approximation up to iterations, keeping $W = W_0$ and updating the Green's function, $G_0 \rightarrow G$, to obtain the so-called GW_0 approximation [36,37]. This approach yields sufficiently better QP energies and spectral properties than the fully self-consistent GW description [35–37]. During these calculations, we have utilized 450 bands, 80 points for the frequency calculations, and 80 eV energy cutoff for the response function. These criteria were established for equally describing the electronic states of the systems [35,38].

3. Results and discussion

To perform a systematic comparison considering the distinct subclasses of oligosilanes, we firstly analyze the structural, electronic and optical properties of the three $Si_x(CH_3)_y$ archetypes, namely tetramethylsilane (TMS), octamethylcyclotetrasilane, and octamethyloctasilacubane displayed in Fig. 1. Their optimized geometries were determined by using as initial structural guess the experimentally available geometric data for these molecules in the gas phase. The parameters of the optimized geometries resulting from our calculations agree well with previously reported data for the same and for analogous molecules in Refs. [22, 39, 40] (see Table 1). As expected

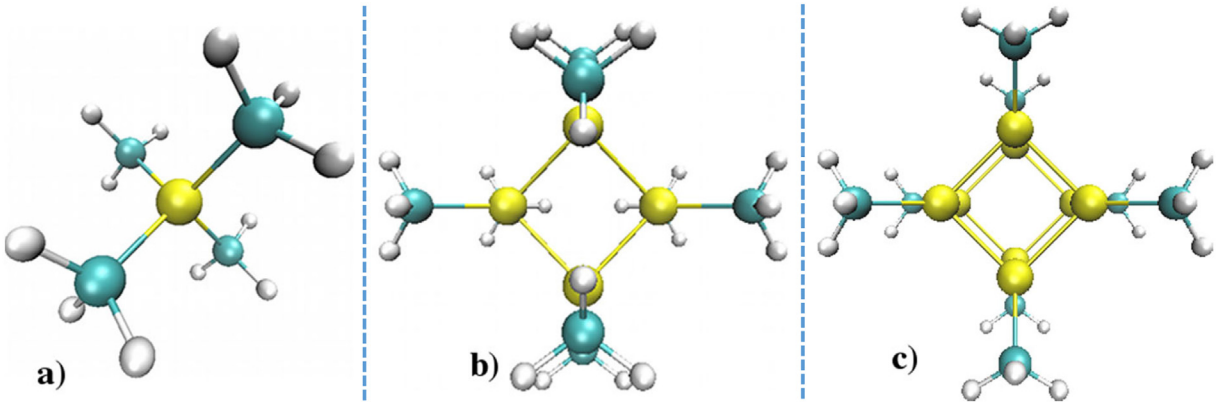

Fig. 1. Optimized geometries of the three oligosilanes as obtained at the LSDA/PAW level of calculation: a) $Si(CH_3)_4$ (TMS); b) $Si_4(CH_3)_8$ (octamethylcyclotetrasilane); and c) $Si_8(CH_3)_8$ (octamethyloctasilacubane).

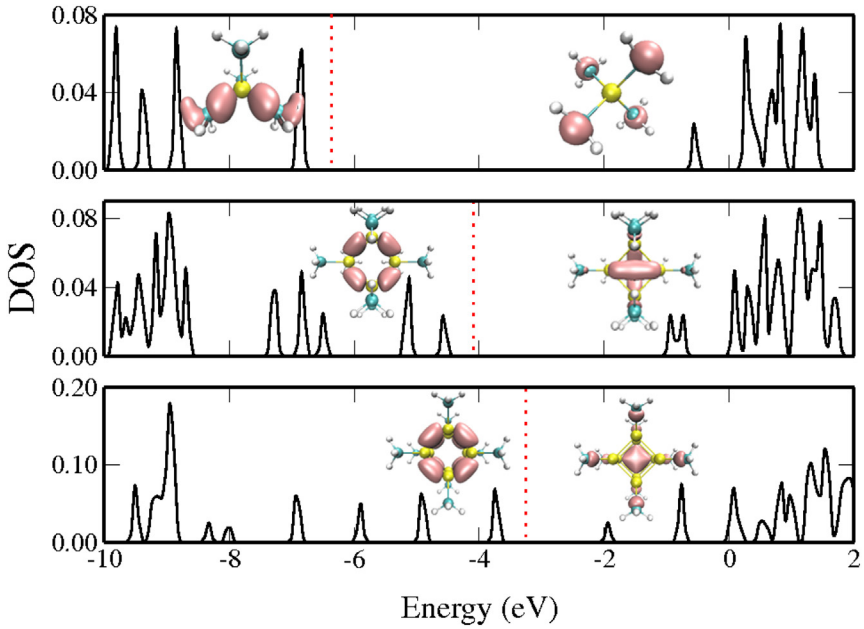

Fig. 2. Calculated DOS (LSDA/PAW) in arbitrary units for $Si(CH_3)_4$ (top panel), $Si_4(CH_3)_8$ (middle panel), and $Si_8(CH_3)_8$ (bottom panel). The KS charge densities of the HOMO (left side) and LUMO (right side) are also shown in the panels. Vertical dashed lines indicate the Fermi energy.

for this sub-class of compounds, the characteristic Si—C bond length value does not vary significantly between the three molecules studied here. A similar trend applies to the Si—Si bond length, when the $Si_4(CH_3)_4$ and the $Si_8(CH_3)_8$ optimized geometries are compared to each other. Moreover, our calculated Si—Si bond length values (2.34–2.37 Å) agree well with the value of 2.36 Å as obtained from gas electron diffraction for octamethylcyclotetrasilane [22].

As we will discuss in the following, these structural parameters reflect the nature of the chemical bond in Si-C-based molecules, clusters, and nanoparticles. While correlation between their structural parameters and their electronic and optical properties is not easily identifiable, the resulting peculiar geometries exhibiting typical electron density distributions are more directly related to the absorption spectra of these oligosilanes.

Fig. 2 displays the calculated density of electronic states (DOS) for the three $Si_x(CH_3)_y$ oligosilanes (cf. the optimized structures in Fig. 1). The KS charge density of the frontier molecular orbitals, i.e., the highest occupied (HOMO) and lowest unoccupied (LUMO) calculated at the Γ point of the BZ, are also shown in the panels of Fig. 2. Considering the simple $Si(CH_3)_4$ oligosilane as a reference system for our calculations, the LSDA/PAW frontier charge densities are in good agreement with those obtained at the generalized gradient approximation (GGA) level of theory, performed for small hydrogenated silicon nanoclusters [41]. At this point, it is noteworthy to point out that the PAW is an adequate method that gives access to the full electron density, and it is adjusted to work efficiently even under low cutoff energy values. The comparison to the results in Ref. [41] ensures that we provide a reliable analysis of the $Si_4(CH_3)_8$ and $Si_8(CH_3)_8$ electron densities, which are scarcely reported in the literature but certainly important to compute optical properties of these molecules. As discernible in Fig. 2 (middle and bottom panels) the square modulus of the HOMOs for these cyclic oligosilanes are delocalized between the Si—Si σ-bonds themselves, whereas the square modulus of the LUMOs are delocalized inside the ring or cage formed by the Si atoms, leading to characteristic $\sigma \rightarrow \sigma^*$ electronic transitions that absorb light at specific frequencies [8,11,18]. These results are appealing in the context of Si-based molecular optical sensing technology that requires chemically stable candidate compounds with adequate optical properties to be employed as efficient optical tags [12].

Now, we report our theoretical results for the optimized geometries of the two persilastaffanes, i.e., persila[1]staffaneane and persila[2] staffaneane, as displayed in Fig. 3. We note that the structure of persila [1]staffaneane forms a Si cage that is, to some extent, comparable to the structures of $Si_4(CH_3)_8$ and $Si_8(CH_3)_8$. Hence, we presume that the typical Si—C and Si—Si bond lengths in persilastaffanes $Si_xH_6(CH_3)_y$ are similar to those in the $Si_x(CH_3)_y$ oligosilanes. The calculated bond lengths reported in Tables 1 and 2 confirm this assumption. More importantly, for $Si_7H_6(CH_3)_6$ and $Si_{12}H_6(CH_3)_{12}$, the optimized geometries obtained with LDA/PAW agree with the available experimental data [11].

As firstly reported by Iwamoto et al. [11], persilastaffanes form highly symmetric rodlike structures containing bicyclo[1.1.1] pentasilane units catenated at the bridgehead positions, as displayed in Fig. 3b. For the persilastaffanes studied here, we obtain that both

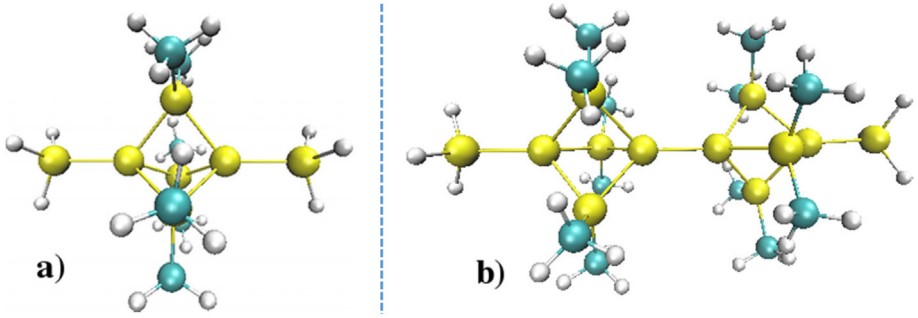

Fig. 3. Optimized geometries of the two persilastaffanes obtained at the LSDA/PAW level of calculation: a) $Si_7H_6(CH_3)_6$ (persila[1]staffaneane); and b) $Si_{12}H_6(CH_3)_{12}$ (persila[2]staffane).

Table 2
Calculated bond lengths for the relaxed persilastaffanes at the LSDA/PAW level of calculation. The experimental values (given in parentheses) are from Ref. [11].

Compound	Si–C (Å)	Si–Si[a] (Å)	Si–Si[b] (Å)	Si–Si[c] (Å)
$Si_7H_6(CH_3)_6$	1.86	2.34 (2.362)	2.31 (2.343)	–
$Si_{12}H_6(CH_3)_{12}$	1.89	2.37 (2.379)	2.34 (2.341)	2.34 (2.360)

[a] Si-ring/cage atoms.
[b] Extremity atoms.
[c] Bridgehead atoms.

Table 3
Calculated HOMO-LUMO energy gaps (DFT) and residual dipole moments (RDM) with LSDA/PAW for all oligosilanes. The optical gaps obtained in the GWA (GW_0) are also reported.

Compound	DFT gap (eV)	RDM (D)	GW_0 gap (eV)
$Si(CH_3)_4$	6.32	0.00	10.18
$Si_4(CH_3)_8$	3.63	0.01	8.28
$Si_8(CH_3)_8$	1.79	0.03	5.44
$Si_7H_6(CH_3)_6$	4.00	0.03	7.72
$Si_{12}H_6(CH_3)_{12}$	3.52	0.11	6.82

the Si—C bond lengths (exhibiting a maximum variation of 1.6%) and the Si—Si bond lengths (exhibiting a maximum variation of 2.6%) tend to be very similar to the corresponding values of $Si_4(CH_3)_8$ and $Si_8(CH_3)_8$ (see Tables 1 and 2). In terms of the electronic structure, however, the persilastaffanes exhibit a σ-delocalization along the silicon cages that implies a reduction of their energy gap when the size of the molecules increases. We refer to this effect further in the discussion about their optical gaps.

The calculated DOS of persila[1]staffaneane and persila[2]staffaneane (cf. optimized geometries in Fig. 3) are displayed in Fig. 4, along with the KS charge densities of the HOMO and LUMO. As illustrated in Fig. 4, when the molecule increases by a bicyclo[1.1.1]pentasilane unit, the occupied KS states spread to higher energies: from less than −5 eV, in the case of $Si_7H_6(CH_3)_6$, to above −4 eV, in the case of $Si_{12}H_6(CH_3)_{12}$. In addition, the shift of the unoccupied KS states to higher energies amounts to less than 0.5 eV. Consequently, these states will contribute in a subtly different way to the optical absorption of the two persilastaffanes. For these two persilastaffanes, the KS charge density of the HOMOs resemble the electronic distribution of the cyclic oligosilanes (see Fig. 2), i.e., they are delocalized on bonded Si atoms in the bicyclo[1.1.1]pentasilane cage, thus giving rise to σ_{cage} orbitals. Nevertheless, the charge densities of the LUMOs of persilastaffanes (as compared to the LUMOs of the cyclic oligosilanes) are more distributed around terminal and bridgehead Si atoms, thus giving rise to σ^*_{axis} orbitals [11]. The differences in the DOS (Fig. 4) are expected to affect the optical absorption profile of these two persilastaffanes, when compared to the absorption spectra of the cyclic oligosilanes. Furthermore, this analysis indicates that the effect of σ-electron delocalization may influence differently the respective absorption spectra of the persilastaffanes and the cyclic oligosilanes.

Before presenting the quasiparticle calculations within the GWA and discussing the optical absorption of the two sub-classes of oligosilanes, in Table 3 we summarize their HOMO-LUMO energy gaps obtained with LSDA/PAW, and their optical gaps obtained with GW_0. In Table 3 we also report the residual dipole moments (RDM) calculated with LSDA/PAW, since RDM permits to gauge small distortions in the symmetric geometries of the molecules, resulting from the optimization process and the electronic structure calculation level. As expected, for the highly symmetric molecules, the RDM values are negligible (0.00–0.03 D). The largest geometric distortion, leading to a small charge separation (RDM = 0.11 D) is observed in the case of $Si_{12}H_6(CH_3)_{12}$, which contains a one-dimensional Si–Si bridge, allowing for small rotations or re-orientations between neighboring Si cages. We also cannot rule out that there is a small effect of the box size in this latter case, as already mentioned here. Certainly, the charge distribution in these molecules can influence their optical properties.

As expected for the $Si_x(CH_3)_y$ sub-class of oligosilanes, with the increase of the molecular volume and the Si concentration, the calculated HOMO-LUMO gaps dramatically decrease, from 6.32 eV, for $Si(CH_3)_4$, to 1.79 eV, for $Si_8(CH_3)_8$ (see Table 3). For the two persilastaffanes, however, we observe a much weaker trend of the HOMO-LUMO gaps that decrease with the molecular size, i.e., from 4.00 eV to 3.52 eV. In Ref. [11], the calculated HOMO-LUMO energy gaps for $Si_7H_6(CH_3)_6$ and for $Si_{12}H_6(CH_3)_{12}$, at the B3LYP/def2-TZVP//B3LYP/6-31G(d) level of theory are, respectively, 5.5 and 4.9 eV. Indeed, hybrid functionals, such as

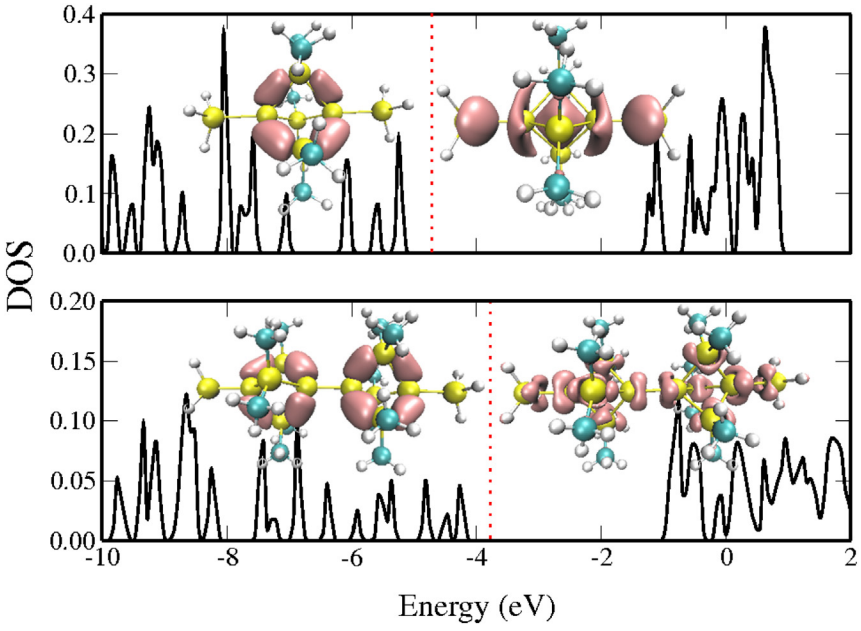

Fig. 4. Calculated DOS (LSDA/PAW) in arbitrary units for $Si_{12}H_6(CH_3)_{12}$ (top panel), and $Si_7H_6(CH_3)_6$ (bottom panel). The KS charge densities of HOMO (left side) and LUMO (right side) are also shown in the panels. Vertical dashed lines indicate the Fermi energy.

B3LYP, are known to yield larger HOMO-LUMO gaps than LSDA or pure GGA, both of which tend to underestimate this value; in any case at the KS-DFT level none of these levels of theory are taking into account the optical gap of the molecules. Thus, we use LSDA here as a method to readily reach a many-body description of the systems and determine the electronic excitations by solving the QP self-consistent equations. For this reason, we proceed up to the GWA to calculate the optical gaps of these systems. This scheme is discussed in more detail in the following paragraphs.

As usual in the GWA, the screened Coulomb interaction W is calculated within the RPA or the Hartree approximation. In the scheme implemented in the VASP code [36,37], this is performed by including local field effects combined with the PAW method [34]. For the purpose of the present study, it is interesting to examine first such effects in the energy excitations of the oligosilanes. In Fig. 5, we display the resulting absorption spectra in terms of the dynamic polarizabilities calculated within the RPA for the $Si_x(CH_3)_y$ oligosilanes (Fig. 5a), and for the $Si_xH_6(CH_3)_y$ persilastaffanes (Fig. 5b). From these calculated spectra, we observe the specific features in the absorptions of each molecule. For example, in the case of $Si(CH_3)_4$ we notice a small absorption band centered at 6.3 eV and a more pronounced absorption band occurring around 7.6 eV. Of course, these absorption peaks are still red shifted with respect to the corresponding values calculated by including microscopically the screening of the Coulomb interaction. Adopting such approach, a more accurate description of the optical gaps is attained after the self-consistency in G having W fixed from the RPA, i.e., $W = W_0$ (see the calculated GW_0 gaps in Table 3).

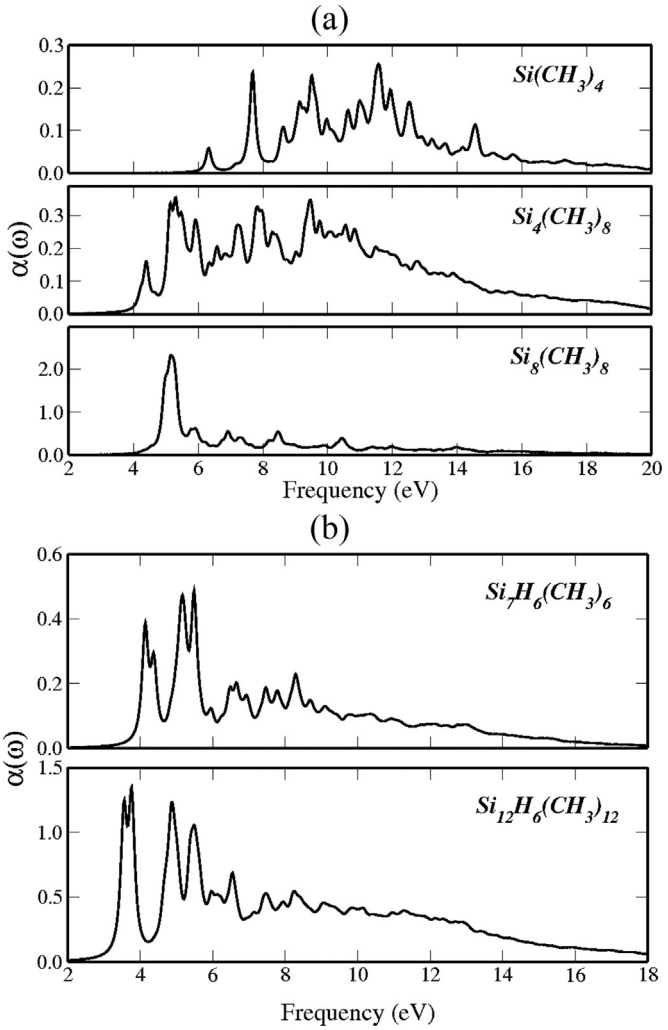

Fig. 5. Calculated RPA absorption spectra expressed in terms of the dynamic polarizabilities (in arbitrary units) for (a) $Si_x(CH_3)_y$ oligosilanes and (b) $Si_xH_6(CH_3)_y$ persilastaffanes.

In the case of $Si_4(CH_3)_8$, we observe the RPA absorptions starting at 4 eV with the peak centered at 4.3 eV, which is now slightly blue shifted with respect to the calculated HOMO-LUMO gap of 3.63 eV. In the case of $Si_8(CH_3)_8$, the RPA absorption starts above 4 eV and peaks about 5 eV. Again, we notice that when adopting this level of approximation, the absorption of $Si_8(CH_3)_8$ is largely blue shifted from the predicted gap of 1.79 eV, obtained with DFT (Table 3). Considering the RPA absorption features of the two persilastaffanes, we obtain theoretical spectra that are to a larger extent similar to each other. For $Si_7H_6(CH_3)_6$, the absorption starts above 3 eV and reaches its first peak at 4.2 eV. Analogously, for $Si_{12}H_6(CH_3)_{12}$ the absorption starts below 3 eV, with the first peak at 3.5 eV. To be noted that, in the case of these two persilastaffanes, the inclusion of local field effects in the RPA calculations does not shift the bands to higher energies, as observed for the RPA spectra of the cyclic oligosilanes. The optical absorption spectra experimentally obtained in hexane and at room temperature for $Si_7H_6(CH_3)_6$ and $Si_{12}H_6(CH_3)_{12}$, respectively, exhibit a wide band around 5.6 eV and a narrow band around 4.7 eV [11]. Although, the calculated spectra with the RPA (in vacuum and without temperature correction) still systematically underestimate the optical gaps of the five oligosilanes studied here, this is a necessary step to obtain a more accurate modeling of their optical gaps within the GWA.

To improve the description for the optical gaps of these oligosilanes, as reported in Table 3, we perform QP calculations up to the GW_0 approximation. Following this scheme, the correction to the HOMO-LUMO gaps is obtained by calculating the difference between the QP energies (ϵ_n^{QP}) and the LSDA eigenvalues (ϵ_n^{LSDA}), i.e., $\Delta GW = \epsilon_n^{QP} - \epsilon_n^{LSDA}$. The GW corrections to the HOMO and LUMO energies as well as to the HOMO-LUMO gap are reported in Table 4. The results indicate that the calculated red shifts for the HOMOs (ΔGW_{HOMO}) systematically decrease with the increasing number of Si atoms in the oligosilanes, whereas the blue shifts in the LUMOs (ΔGW_{LUMO}) increase more significantly from $Si(CH_3)_4$ to $Si_4(CH_3)_8$, practically remain constant for $Si_8(CH_3)_8$ and $Si_7H_6(CH_3)_6$, and slightly decrease for $Si_{12}H_6(CH_3)_{12}$. These differences produced by the QP calculations significantly open the optical gaps calculated within GWA with values ranging 3.30–4.65 eV, as indicated by the ΔGW_{gap} quantity reported in Table 4. The resulting optical gaps calculated at this level of approximation were already anticipated in the third column of Table 3. It is worth mentioning that, although the GW calculations introduce the screening of the Coulomb interaction in a non-phenomenological way, they can still yield overestimated optical gaps, as observed for $Si_7H_6(CH_3)_6$ and $Si_{12}H_6(CH_3)_{12}$. This overestimation can be attributed to the underestimated screening calculated within the RPA for these two molecules. Furthermore, the lack of electron-hole interactions in the GW method may contribute certain insufficiency to the description of the excitations in persilastaffanes. Notwithstanding, the GWA seems to be an adequate computational procedure to theoretically compute the optical properties of larger oligosilanes and Si-C-based molecules, clusters, and complexes.

In Fig. 6, the GW_0 gap is depicted as a function of the Si concentration, as defined to heavy atoms only: $n_{Si}/(n_{Si} + n_C)$, where n_{Si} is the number of Si atoms and n_C is the number of C atoms, obtained from

Table 4
Quasiparticle corrections to the HOMO and LUMO energies and to the LSDA/PAW gaps for the oligosilanes. The resulting GW_0 gaps are reported in Table 3.

Compound	ΔGW_{HOMO} (eV)	ΔGW_{LUMO} (eV)	ΔGW_{gap} (eV)
$Si(CH_3)_4$	−2.16	1.69	3.86
$Si_4(CH_3)_8$	−1.40	3.24	4.65
$Si_8(CH_3)_8$	−0.89	2.77	3.66
$Si_7H_6(CH_3)_6$	−0.97	2.76	3.72
$Si_{12}H_6(CH_3)_{12}$	−0.75	2.55	3.30

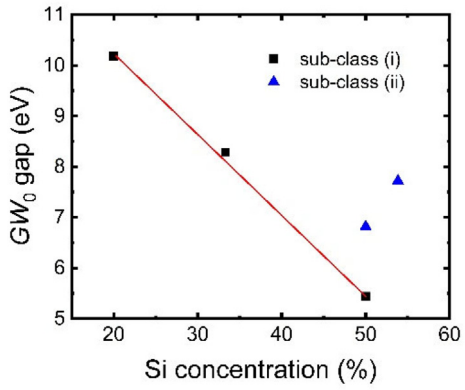

Fig. 6. GW_0 gap as a function of the Si concentration (as defined to heavy atoms only) for the two sub-classes of oligosilanes considered in this study: (i) $Si_x(CH_3)_y$ and (ii) $Si_xH_6(CH_3)_y$.

the stoichiometry of each of the molecules. As seen in Fig. 6, the GW_0 gap for the $Si_x(CH_3)_y$ sub-class of oligosilanes linearly decreases with increasing Si concentration, from 10.18 eV for $Si(CH_3)_4$ to 5.44 eV for $Si_8(CH_3)_8$. In the case of persilastaffanes, i.e., the $Si_xH_6(CH_3)_y$ sub-class of oligosilanes, the dependence of the GW_0 gap on the Si concentration follows the opposite trend, as observed for the $Si_x(CH_3)_y$ oligosilanes. The optical gap of persilastaffanes decreases from 7.72 eV for $Si_7H_6(CH_3)_6$, which exhibits the highest Si concentration of 54%, to 6.82 eV for $Si_{12}H_6(CH_3)_{12}$, which exhibits the lowest Si concentration of 50%. A plausible explanation for this trend, observed for the optical gap of persilastaffanes as a function of their Si concentration resides in the fact that these molecules increase in size as catenated linear structures. Thus, increasingly larger molecules that possess smaller Si concentrations will exhibit smaller band gaps, because of the σ delocalization in the Si cages [11]. These results illustrate the dependence of the optical gap, for distinct oligosilanes, on their molecular size, Si concentration, and type of backbone (i.e., containing Si dots, single rings, single cages, or even multiple cages).

4. Conclusions

We have employed a theoretical protocol based on the many-body GWA to calculate QP excitation energies and investigate the optical properties of Si-C-based molecules: (i) $Si_x(CH_3)_y$ oligosilanes and (ii) $Si_xH_6(CH_3)_y$ persilastaffanes. These stable and synthesizable molecules are valuable prototypes of Si-C-based nanoparticles, with potential applications as efficient light absorbers/emitters in molecular optical devices. Our calculations include local field effects in the RPA for the description of the frequency dependent dielectric response function, going up to the GW_0 approximation. Thus, we have utilized a fully ab initio method, without including a pre-defined amount of screening in the Coulomb interactions of the systems, which is an important ingredient to obtain optical gaps for related molecular systems, such as oligosilanes. Furthermore, this method is partially self-consistent, i.e., updating only *G*, which conserves particle number, yields spectral accuracy, and is computationally less demanding than the fully self-consistent *GW* method.

Our theoretical predictions of the optical absorption properties of oligosilanes within the GWA are in line with their light-absorption characteristic of wide-gap molecules. Moreover, the QP calculations reveal subtle differences in the dependence of the optical gap on their size, Si concentration, and backbone type, for each of the studied sub-classes of oligosilanes. Although the GW_0 level of approximation appears to overestimate the optical gaps of persilastaffanes, this result can be attributed to the underscreening inherent to the RPA and to their characteristic delocalized σ bonds. However, the present methodology is sufficiently flexible to provide realistic optical properties, by recalibrating the exchange-correlation potential in the KS-DFT calculations and re-scaling the *GW* calculations. Therefore, this method is attractive to deal with larger Si-C-based clusters and nanostructures with potential applications in the emerging molecular sensing technology.

CRediT authorship contribution statement

Maria I. A. de Oliveira: performing most for the calculations, researching status of the literature on the subject.

Roberto Rivelino: conceptualization of research, ideas and input about choices and limitations of this project, planning and supervision of most of the calculations, key contribution to interpretation of the calculation results and their validity and perspective, writing initial draft together with Gueorgui Gueorguiev.

Fernando de Brito Mota: Ideas and input about choices of methodology, performing test calculations and defining the best parameters for the present calculations, supervision of part of the calculations.

Anelia Kakanakova-Georgieva: Evaluation of experimental relevance and consulting the comparison to experimental data; its critical interpretation and relevant discussion.

Gueorgui K. Gueorguiev: initial research idea, leadership and conceptualization of research, formulation of research goals and plans. Interpretation of results for the purposes of this manuscript, philosophy, and message of the manuscript in both theoretical and experimental context; writing initial draft together with Roberto Rivelino.

All authors have contributed to the manuscript writing and have read the final version of the manuscript and commented on it.

Declaration of competing interest

The authors declare that they have no known competing financial interests or personal relationships that could have appeared to influence the work reported in this paper.

Acknowledgements

This work was partially supported by the Brazilian agencies Conselho Nacional de Desenvolvimento Científico e Tecnológico (CNPq) and Coordenação de Aperfeiçoamento de Pessoal de Nível Superior - Brasil (CAPES) - Finance Code 001, within the CAPES-PrInt Program. RR also thanks INCT-FCx. GKG and AKG acknowledge the support by the Swedish Research Council (VR) through VR 2017-04071. GKG further acknowledges the support by Åforsk through grant 18-266.

References

[1] Z. Huang, M.L. Tang, Semiconductor nanocrystal light absorbers for photon upconversion, J. Phys. Chem. Lett. 9 (2018) 6198–6206.
[2] N. Nishimura, J.R. Allardice, J. Xiao, Q. Gu, V. Gray, A. Rao, Photon upconversion utilizing energy beyond the band gap of crystalline silicon with a hybrid TES-ADT/PbS quantum dots system, Chem. Sci. 10 (2019) 4750–4760.
[3] A.J. Pearson, T. Plint, S.T.E. Jones, B.H. Lessard, D. Credgington, T.P. Bender, N.C. Greenham, Silicon phthalocyanines as dopant red emitters for efficient solution processed OLEDs, J. Mater. Chem. C 5 (2017) 12688–12698.
[4] M. Philippi, C. You, C.P. Richter, M. Schmidt, J. Thien, D. Lißе, J. Wollschläger, J. Piehler, M. Steinhart, Close-packed silane nanodot arrays by capillary nanostamping coupled with heterocyclic silane ring opening, RSC Adv. 9 (2019) 24742–24750.
[5] J. Teichmann, M. Wagner, Silicon chemistry in zero to three dimensions: from dichlorosilylene to silafullerane, Chem. Commun. 54 (2018) 1397–1412.
[6] G. He, O. Shynkaruk, M.W. Lui, E. Rivard, Small inorganic rings in the 21st century: from fleeting intermediates to novel isolable entities, Chem. Rev. 114 (2014) 7815–7880.
[7] R. West, Cyclic organosilicon compounds. I. Preparation of cyclic silanes, J. Am. Chem. Soc. 76 (1954) 6012–6014.
[8] A. Tsurusaki, C. Iizuka, K. Otsuka, S. Kyushin, Cyclopentasilane-fused hexasilabenzvalene, J. Am. Chem. Soc. 135 (2013) 16340–16343.
[9] A. Bodi, K.L. Sigurdardottir, Á. Kvaran, R. Bjornsson, I. Arnason, Dissociative photoionization of 1-halogenated silacyclohexanes: silicon traps the halogen, J. Phys. Chem. A 120 (2016) 9188–9197.
[10] H. Li, M.H. Garner, Z. Shangguan, Y. Chen, Q. Zheng, T.A. Su, M. Neupane, T. Liu, M.L. Steigerwald, F. Ng, C. Nuckolls, S. Xiao, G.C. Solomon, L. Venkataraman, Large

variations in the single-molecule conductance of cyclic and bicyclic Silanes, J. Am. Chem. Soc. 140 (2018) 15080–15088.
[11] T. Iwamoto, D. Tsushima, E. Kwon, S. Ishida, H. Isobe, Persilastaffanes: design, synthesis, structure, and conjugation between silicon cages, Angew. Chem. Int. Ed. 51 (2012) 2340–2344.
[12] A. Das, P.T. Snee, Synthetic developments of nontoxic quantum dots, ChemPhysChem 17 (2016) 598–617.
[13] L. Albers, S. Rathjen, J. Baumgartner, C. Marschner, T. Müller, Dispersion-energy-driven Wagner–Meerwein rearrangements in oligosilanes, J. Am. Chem. Soc. 138 (2016) 6886–6892.
[14] S. Ishida, K. Otsuka, Y. Toma, S. Kyushin, An organosilicon cluster with an octasilacuneane core: a missing silicon cage motif, Angew. Chem. Int. Ed. 52 (2013) 2507–2510.
[15] T. Iwamoto, S. Ishida, Silicon compounds with inverted geometry around silicon atoms, Chem. Lett. 43 (2014) 164–170.
[16] A. Tsurusaki, S. Kyushin, The radical anion of cyclopentasilane-fused hexasilabenzvalene, Chem. Eur. J. 22 (22) (2016) 134–137.
[17] A. Tsurusaki, Y. Koyama, S. Kyushin, Decasilahexahydrotriquinacene and decasilaisotwistane: σ conjugation on a bowl surface, J. Am. Chem. Soc. 139 (11) (2017) 3982–3985.
[18] Y. Yamaguchi, Electronic structure of polybicyclo[1.1.1]pentasilane, polybicyclo [2.2.2]octasilane, polyoctasilacubane and related compounds, Synth. Met. 62 (1994) 23–26.
[19] N.D. Espinosa-Torres, D. Hernández-de la Luz, J.F.J. Flores-Gracia, J.A. Luna-López, J. Martínez-Juárez, D.E. Vázquez-Valerdi, Evaluation of optical and electronic properties of silicon nano-agglomerates embedded in SRO: applying density functional theory, Nanoscale Res. Lett. 9 (2014) 507.
[20] Y. Kanemitsu, K. Suzuki, M. Kondo, S. Kyushin, H. Matsumoto, Luminescence properties of a cubic silicon cluster octasilacubane, Phys, Rev. B 51 (1995) 10666.
[21] H. Matsumoto, K. Higuchi, Y. Hoshino, H. Koike, Y. Naoi, Y. Nagai, The first octasilacubane system: synthesis of octakis-(t- butyldimethylsilyl)pentacyclo [4.2.0.$0^{2,5}$.$0^{3,8}$.$0^{4,7}$]octasilane, J. Chem. Soc., Chem. Commun. (1988) 1083–1084.
[22] V.S. Mastryukov, S.A. Strelkov, L.V. Vilkov, M. Kolonits, B. Rozsondai, H.G. Schuster, E. Henge, The molecular structure of octamethylcyclotetrasilane, $Si_4(CH_3)_8$, from gas electron diffraction, J. Mol. Struct. 238 (1990) 433–437.
[23] Y. Muramatsu, T. Kaneyoshi, Si Kβ X-ray emission spectra of cubic silicon molecules identified by discrete variational (DV) Xα molecular orbital calculations, J. Electron Spectrosc. 107 (2000) 27–32.
[24] R.O. Jones, Density functional theory: its origins, rise to prominence, and future, Rev. Mod. Phys. 87 (2015) 897.
[25] G. Onida, L. Reining, A. Rubio, Electronic excitations: density-functional versus many-body Green's-function approaches, Rev. Mod. Phys. 74 (2002) 601.
[26] Y. Yokouchi, S. Ishida, T. Iwamoto, Facile skeletal rearrangement of polycyclic disilenes with bicyclo[1.1.1]pentasilanyl groups, Chem. Eur. J. 24 (2018) 11393–11401.
[27] J.P. Perdew, A. Zunger, Self-interaction correction to density-functional approximations for many-electron systems, Phys. Rev. B 23 (1981) 5048.
[28] G. Kresse, J. Hafner, Ab initio molecular dynamics for liquid metals, Phys. Rev. B 47 (1993) 558.
[29] G. Kresse, J. Hafner, Ab initio molecular-dynamics simulation of the liquid-metal-amorphous-semiconductor transition in germanium, Phys. Rev. B 49 (1994) 14251.
[30] G. Kresse, J. Furthmüller, Efficiency of ab-initio total energy calculations for metals and semiconductors using a plane-wave basis set, Comput. Mater. Sci. 6 (1996) 15–50.
[31] G. Kresse, J. Furthmüller, Efficient iterative schemes for ab initio total-energy calculations using a plane-wave basis set, Phys. Rev. B 54 (1996) 11169.
[32] P.E. Blöchl, Projector augmented-wave method, Phys. Rev. B 50 (1994) 17953.
[33] G. Kresse, D. Joubert, From ultrasoft pseudopotentials to the projector augmented-wave method, Phys. Rev. B 59 (1999) 1758.
[34] M. Gajdos, K. Hummer, G. Kresse, Linear optical properties in the projector-augmented wave methodology, Phys. Rev. B 73 (2006), 045112, .
[35] C. Franchini, A. Sanna, M. Marsman, G. Kresse, Structural, vibrational, and quasiparticle properties of the Peierls semiconductor $BaBiO_3$: a hybrid functional and self-consistent *GW* + vertex-corrections study, Phys. Rev. B 81 (2010), 085213, .
[36] M.S. Hybertsen, S.G. Louie, Electron correlation in semiconductors and insulators: band gaps and quasiparticle energies, Phys. Rev. B 34 (1986) 5390.
[37] M. Shishkin, G. Kresse, Self-consistent *GW* calculations for semiconductors and insulators, Phys. Rev. B 75 (2007) 235102.
[38] M.I.A. Oliveira, R. Rivelino, F.B. Mota, G.K. Gueorguiev, Optical properties and quasiparticle band gaps of transition-metal atoms encapsulated by silicon cages, J. Phys. Chem. C 118 (2014) 5501–5509.
[39] K. Shimizu, H. Murata, Normal vibrations and calculated thermodynamic properties of tetramethylsilane, J. Mol. Spectrosc. 5 (1961) 44–51.
[40] A.R. Campanelli, F. Ramondo, A. Domenicano, I. Hargittai, Toward a more accurate silicon stereochemistry: an electron diffraction study of the molecular structure of tetramethylsilane, Struct. Chem. 11 (2000) 155–160.
[41] E. Degoli, G. Cantele, E. Luppi, R. Magri, D. Ninno, O. Bisi, S. Ossicini, Ab initio structural and electronic properties of hydrogenated silicon nanoclusters in the ground and excited state, Phys. Rev. B 69 (2004) 155411.